Strength Deterioration and Degradation Mechanism of Glass Chopped Reinforced Plastics in Water Environment*

Hideki SEKINE**, Keiichi SHIMOMURA**
and Norio HAMANA***

In this paper the effect of water environment on the fracture toughness of glass chopped strand reinforced plastics is discussed. Fracture toughness tests were performed by using compact tension specimens of the composite immersed in distilled water for 10 days to 1.5 years. Acoustic emission signals were detected during the tests. The observation of fracture surfaces by a SEM and the quantitative analysis of dissolution elements from glass fibers by an atomic absorption spectrophotometer were also carried out to clarify the degradation mechanism of the composite. It was found that (1) the fracture toughness obtained by the acoustic emission method decreases as the immersion time is longer; (2) the decrease of the fracture toughness is caused by the degradation of the bonding interface between glass fibers and the resin matrix and the weakening of glass fibers due to the dissolution of the elements in water.

Key Words: Composite Materials, GFRP, Fracture Toughness, Water Environment, Degradation, AE

1. Introduction

With the increasing use of fiber-reinforced plastics (FRP) as structural components in water and corrosive environments, the study of the effect of the environments on the strength and fracture toughness of FRP has received wide attention. The effects of water and moisture on the mechanical properties of FRP have been studied by many investigators[1]~[4]. They have shown that the strength, fracture toughness and fatigue crack growth resistance decrease remarkably due to the absorption of water and moisture. Although the absorption of water is dependent on the specimen geometry and the material, investigators have not discussed the problem by using an adequate parameter characterizing the water absorption.

It is well known that the load-deflection curves obtained from the fracture toughness tests of FRP usually indicate nonlinear behavior and that there is no macroscopic crack initiation such as the pop-in phenomenon of metals. The exact evaluation of the fracture toughness of FRP has been extensively discussed[3]~[5]. Recently, the authors and co-workers[6]~[8] have applied the acoustic emission (AE) technique to determine the fracture toughness of FRP. The AE signals during the fracture toughness tests correspond to the microfracture, i. e., resin cracking, fiber debonding and fiber breakage. It is found that the value of fracture toughness K_{AE}, which is defined as a critical stress intensity factor at a load with the abrupt increase of AE energy, agrees satisfactorily with the value of the fracture toughness obtained by means of the 5% offset procedure of the ASTM Standard[9].

The degradation mechanism of resin, fiber and interface between fiber and matrix due to water and acid environments has been reviewed and discussed thus far[10][11]. From the detailed observation and X-ray analysis of the fractured surface, it is found that the elements Al, Ca, K and Na are removed from the FRP due to immersion.

In this paper, the fracture toughness tests were

* Received 2nd February, 1988. Paper No. 86-0340 A
** Faculty of Engineering, Tohoku University, Aramaki Aza Aoba, Sendai, 980, Japan
*** Tokyo Electric Power Co., Inc., 1-1-3 Uchisaiwai-chou, Chiyoda-ku, Tokyo, 100, Japan

performed by means of the AE method for a random short-fiber sheet molding compound composite immersed in water. The effect of water on the fracture toughness of the FRP is discussed. Moreover, a quantitative analysis of dissolution elements from the FRP was carried out, and the degradation mechanism of the FRP in water is discussed.

2. Material and Experimental Procedure

2.1 Material

The material is a random short-fiber sheet molding compound composite RCM-312-25 which contains E-glass fibers of 60±2% by weight in an unsaturated polyester resin matrix. The chopped fiber strands consist of 400 E-glass fibers of 13 μm diameter and 25.4 mm length. The FRP was made as a laminate with 8 layers, which is cured for 9 minutes at 125°C and under a pressure of 5.9 MPa.

2.2 Fracture toughness tests

The fracture toughness tests were performed using the compact tension specimens, as shown in Fig. 1. The notch root radius ρ is 0.25 mm. The specimens were put in a desiccator containing silica gel ($SiO_2 \cdot nH_2O$) for 1 month. After that, the specimens were immersed in distilled water at a temperature of 25±0.1°C for 10, 30, 60 or 90 days, or 1 year. Experiments were conducted on the specimens in water bath at 25±0.1°C, utilizing a screw-driven testing machine. The crosshead speed was kept at 0.3 mm/min throughout the tests. The relationship between the load P and the crack mouth displacement V_M was recorded in an X-Y recorder. The AE signals were detected by an AE transducer (NF Corp. AE 905 S) with a resonant frequency of 1 MHz. The transducer was connected to the end of a stainless waveguide of 200 mm length and 4 mm diameter (Fig. 1). The AE signals from the transducer were recorded on a VTR type recorder (Sony FMR-1219) for the data analysis of AE energy $V^{2(12)}$.

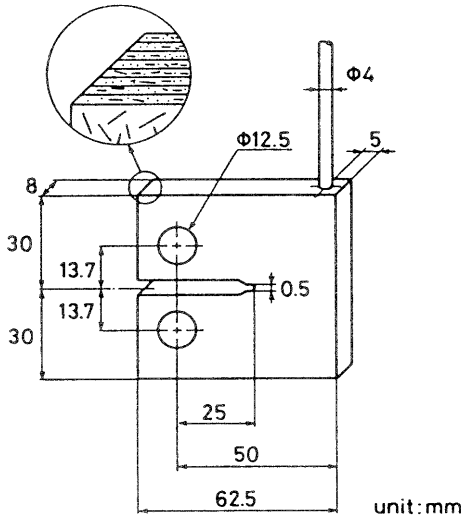

Fig. 1 Geometry of compact tension specimens

2.3 Quantitative analysis of dissolution elements

The dissolution elements from the FRP were examined by an atomic absorption spectrophotometer to clarify the degradation mechanism of the FRP in water. Al, Ca, Mg, B, K and Na content was analyzed.

3. Transient Behavior of Water Absorption in a Crack Tip Region

3.1 Diffusion coefficient and saturated weight of water

After a specimen had been immersed in dilute red ink for 10 days, a colored region was observed. The edge surface showed a maximum color depth of about 2 mm, while the specimen surface perpendicular to the plane showed no obvious coloration. This indicates that water easily diffuses into this specimen in the plane.

Consider a rectangular plate specimen ($0<x, y<a, 0<z<b$) as shown in Fig. 2. When the water absorption is constant throughout the thickness of the specimen, the diffusion problem of water reduces to a two-dimensional one. Then, the diffusion equation is written as

$$\frac{\partial C}{\partial t}=D\left(\frac{\partial^2 C}{\partial x^2}+\frac{\partial^2 C}{\partial y^2}\right), \tag{1}$$

where C is the weight of water absorbed per unit volume, D the diffusion coefficient and t the immersion period. The weight of water C is assumed to be zero initially throughout the specimen. When the specimen is immersed in water at time $t=0$, the initial and boundary conditions are given by

$$C(x, y, 0)=0\ ;\ t=0 \tag{2}$$

$$\left.\begin{aligned} &C(0, y, t)=C_s\\ &C(a, y, t)=C_s\\ &C(x, 0, t)=C_s\\ &C(x, a, t)=C_s \end{aligned}\right\}\ ;\ 0\leqq x, y\leqq a,\ t>0, \tag{3}$$

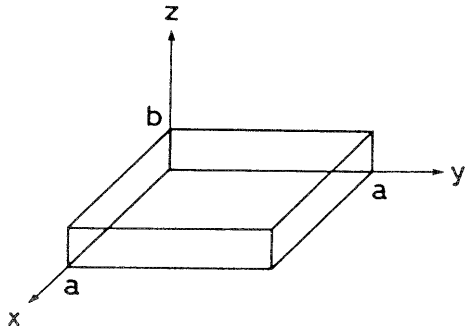

Fig. 2 Rectangular plate specimen and coordinate system for water absorption test

where C_s is the saturated weight of water. The Fourier series solution[13] of Eq.(1) satisfying Eqs.(2) and (3) is obtained as follows:

$$C(x, y, t)=C_s\Big[1-\frac{16}{\pi^2}\times\sum_{m=0}^{\infty}\sum_{n=0}^{\infty}\frac{\exp\Big\{-\pi^2 D\frac{(2m+1)^2+(2n+1)^2}{a^2}t\Big\}}{(2m+1)^2(2n+1)^2}\times\sin\frac{(2m+1)}{a}x\cdot\cos\frac{(2n+1)}{a}y\Big] \quad (4)$$

Integrating Eq.(4) with respect to x and y, the total weight of water absorbed in the specimen W_0 is written as

$$W_0(t)=a^2bC_s\Big[1-\frac{64}{\pi^4}\times\sum_{m=0}^{\infty}\sum_{n=0}^{\infty}\frac{\exp\Big\{-\pi^2 D\frac{(2m+1)^2+(2n+1)^2}{a^2}t\Big\}}{(2m+1)^2(2n+1)^2}\Big] \quad (5)$$

The weight of water absorbed in the specimen during the test is shown in Fig. 3. The solid circles are the results of the specimen having the dimensions of $a=68.3$ mm and $b=8$ mm. In order to determine the values of the diffusion coefficient D and the saturated weight of water C_s, Eq.(5) was fitted to the experimental results by the least mean square method. The values were obtained as $D=9.38\times10^{-12}$ m^2/s and $C_s=8.51$ kg/m^3. The solid line in Fig. 3 is the weight of water W_0 which is calculated by substituting the values of D and C_s into Eq.(5). It is found that the calculated result agrees satisfactorily with the experimental results.

3.2 Average weight of water in a circle region near the crack tip

The water absorption in the region near the crack tip may remarkably affect the fracture toughness. Now, let us consider the weight of water which is absorbed from the surfaces of a crack of length $2l$ in an infinite body, as shown in Fig. 4. This analysis may be valid to estimate the water absorption in the region near the crack tip, when the compact tension specimen of crack length l is immersed in distilled water. Again, the weight of water C is assumed to be zero initially. The initial and boundary conditions are given by

$$C(x, y, 0)=0;\ t=0 \quad (6)$$

$$C(x, 0, t)=C_s;\ |x|<l,\ t>0 \quad (7)$$

By using the solution for a point heat source in an infinite medium[14], the weight of water is written as

$$C(x, y, t)=\frac{1}{4\pi D}\int_0^t\int_{-l}^{l}\frac{Q(s, \bar{t})}{t-\bar{t}}\times\exp\Big\{-\frac{(x-s)^2+y^2}{4D(t-\bar{t})}\Big\}ds d\bar{t} \quad (8)$$

where $Q(s, t)$ is the weight of water absorbed at a point $(x=s, y=0)$ per unit time of t. Substitution of Eq.(8) into Eq.(7) yields

$$\frac{1}{\pi}\int_0^T\int_{-1}^{1}\frac{G(S, \bar{T})}{T-\bar{T}}\exp\Big\{-\frac{(X-S)^2}{4(T-\bar{T})}\Big\}dS d\bar{T}=4C_s;\ |X|<1,\ T>0 \quad (9)$$

where

$$X=x/l,\ S=s/l,\ T=Dt/l^2,\ \bar{T}=D\bar{t}/l^2,\ G(S, \bar{T})=lQ(s, \bar{t})/D \quad (10)$$

Here, the singular integral equation (9) is solved effectively by means of the collocation method. We divide the interval $[0, T]$ with respect to $\bar{T}$ into M parts, and the interval $[-1, 1]$ with respect to S into N parts. It is assumed that the density function $G(S, \bar{T})$ is uniform in each part of the interval. Then the simultaneous linear equation is obtained from Eq.(9) as follows:

$$\sum_{i=1}^{j}\sum_{\xi=1}^{N}G(X_\xi, \bar{T}_i)\int_{\bar{T}_{i-1}}^{\bar{T}_i}\int_{S_{\xi-1}}^{S_\xi}\frac{1}{\bar{T}_j-\bar{T}}\times\exp\Big\{-\frac{(X_\eta-S)^2}{4(\bar{T}_j-\bar{T})}\Big\}dS d\bar{T}=-4\pi C_s$$
$$j=1, 2, \cdots, M,\quad \eta=1, 2, \cdots, N, \quad (11)$$

where the collocation points X_η and the separate points S_ξ have been chosen such that

$$X_\eta=\cos\Big(\frac{\pi\eta}{N+1}\Big),\quad S_\xi=\cos\Big(\frac{\pi\xi}{N}\Big). \quad (12)$$

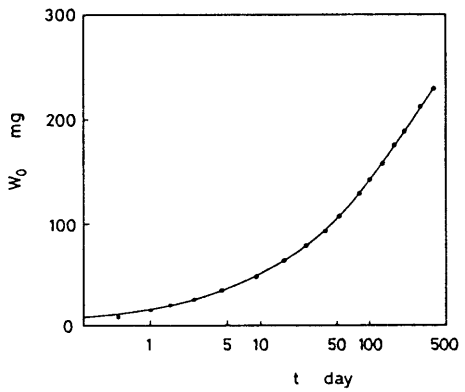

Fig. 3 Weight of water against immersion time

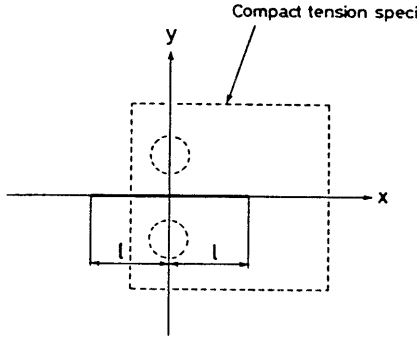

Fig. 4 Compact tension specimen with notch of length l and two-dimensional crack of length $2l$ in an infinite body

The double integrals in Eq.(11) are easily expressed analytically as follows:

$$\int_{\bar{T}_{i-1}}^{\bar{T}_i}\int_{S_{\xi-1}}^{S_\xi}\frac{1}{\bar{T}_j-\bar{T}}\exp\left\{-\frac{(X_\eta-S)^2}{4(\bar{T}_j-\bar{T})}\right\}dSd\bar{T}$$
$$=2\{\pi(\bar{T}_j-\bar{T}_{i-1})\}^{1/2}\left[\mathrm{erf}\left\{\frac{X_\eta-S_{\xi-1}}{2(\bar{T}_j-\bar{T}_{i-1})^{1/2}}\right\}\right.$$
$$\left.-\mathrm{erf}\left\{\frac{X_\eta-S_\xi}{2(\bar{T}_j-\bar{T}_{i-1})^{1/2}}\right\}\right]-2\{\pi(\bar{T}_j-\bar{T}_i)\}^{1/2}$$
$$\times\left[\mathrm{erf}\left\{\frac{X_\eta-S_{\xi-1}}{2(\bar{T}_j-\bar{T}_i)^{1/2}}\right\}-\mathrm{erf}\left\{\frac{X_\eta-S_\xi}{2(\bar{T}_j-\bar{T}_i)^{1/2}}\right\}\right]$$
$$+(X_\eta-S_\xi)\left[\mathrm{E}_i\left\{-\frac{(X_\eta-S_\xi)^2}{4(\bar{T}_j-\bar{T}_{i-1})}\right.\right.$$
$$\left.\left.-\mathrm{E}_i\left\{-\frac{(X_\eta-S_\xi)^2}{4(\bar{T}_j-\bar{T}_i)}\right\}\right]-(X_\eta\right.$$
$$\left.-S_{\xi-1})\left[\mathrm{E}_i\left\{-\frac{(X_\eta-S_{\xi-1})^2}{4(\bar{T}_j-\bar{T}_{i-1})}\right\}\right.\right.$$
$$\left.\left.-\mathrm{E}_i\left\{-\frac{(X_\eta-S_{\xi-1})^2}{4(\bar{T}_j-\bar{T}_i)}\right\}\right],\qquad(13)$$

where $\mathrm{erf}(x)$ is the error function and $\mathrm{E}_i(x)$ is the exponential integral function.

The weight of water $C(x, y, t)$ can be obtained by substituting the density function $G(S, \bar{T})$ into the following equation.

$$C(x,y,t)=-\frac{1}{4\pi}\sum_{i=1}^{M}\sum_{\xi=1}^{N}G(X_\xi,\bar{T}_i)$$
$$\times\int_{\bar{T}_{i-1}}^{\bar{T}_i}\int_{S_{\xi-1}}^{S_\xi}\frac{l^2}{Dt-l^2\bar{T}}$$
$$\times\exp\left\{-\frac{(x-lS)^2+y^2}{4(Dt-l^2\bar{T})}\right\}dSd\bar{T}.\qquad(14)$$

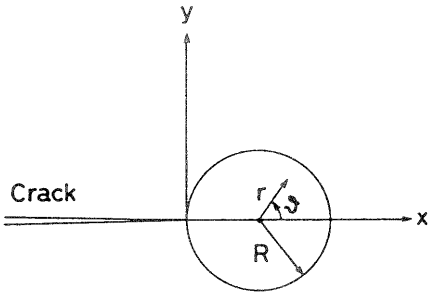

Fig. 5 Circle of radius R adjacent to the crack tip

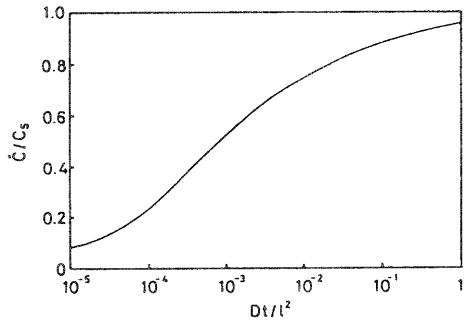

Fig. 6 Average weight of water absorbed in the circle adjacent to the crack tip against immersion time

Consider an average weight of water absorbed in the region near the crack tip to assess the deterioration of fracture toughness in water. The average weight of water C absorbed in the circle of a radius R adjacent to the crack tip is given by using the weight of C (Fig. 5), such that

$$\hat{C}=\frac{1}{\pi R^2}\int_0^{2\pi}\int_0^R Crdrd\theta.\qquad(15)$$

In the calculation of Eq.(15), the radius R is set as $R/l=0.02$ because the 5% offset from the linear compliance on the P-V_M record corresponds to the crack extension by 2% of the initial crack length. The average weight of water $\hat{C}/C_s$ against time is shown in Fig. 6.

4. Results of Fracture Toughness

Figure 7 shows the load P-crack mouth displacement V_M curves for the specimens immersed in distilled water for 10, 30, 60 and 90 days, for 1 year, and for a specimen without immersion. It is seen that the P-V_M curves indicate different behavior between the specimens immersed in water and those not immersed. The P-V_M curves for the immersed specimens show more significant nonlinear behavior before the maximum load than that for the nonimmersed specimen. The ability to bear the load decreases with increasing immersion time, such that the maximum load is 3.42 kN for no immersion time, 2.82 kN for 90 days and 2.04 kN for 1 year. Beyond the maximum load, the load

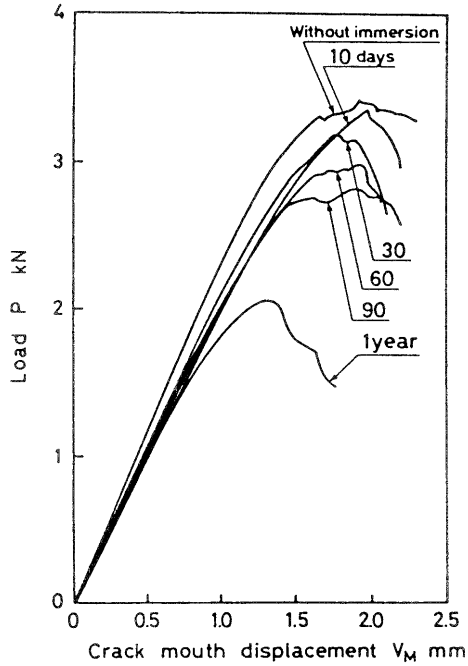

Fig. 7 P-V_M curves for the specimens immersed in distilled water for 10, 30, 60 and 90 days, for 1 year, and for a specimen without immersion

P drops gradually for the specimen without immersion, while the load drops abruptly for the immersed specimen.

Figures 8 and 9 show the number of AE events together with the P-V_M curves for the specimen without immersion and the specimen immersed for 1 year, respectively. The AE data are shown as the number of AE events detected for a 5-second interval, whose peak amplitude is greater than 0.2 V at the gain of 50 dB. It is seen that the number of AE events

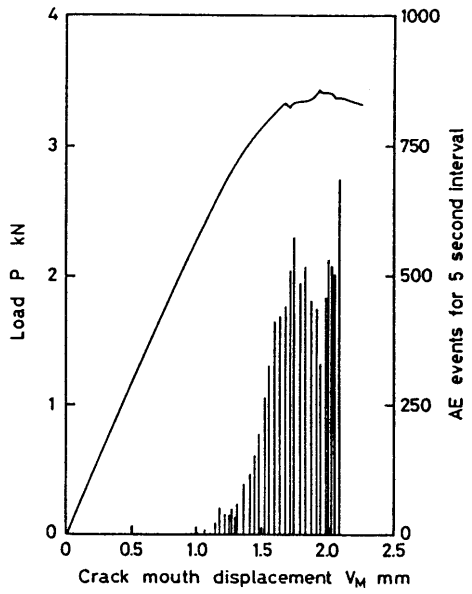

Fig. 8 Number of AE events for a 5-second interval and P-V_M curve for the specimen without immersion

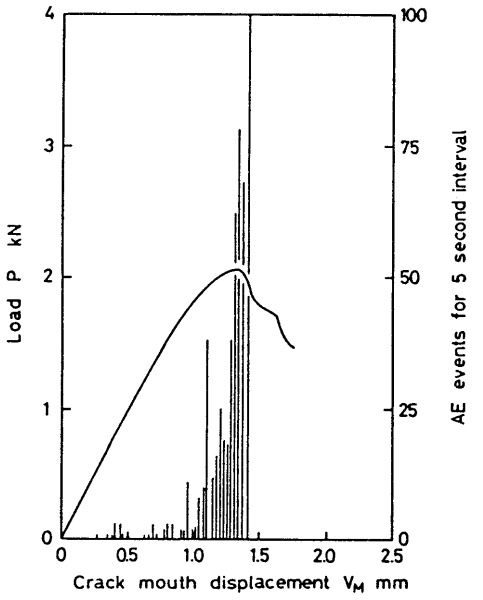

Fig. 9 P-V_M curve and number of AE events for a 5-second interval for the specimen immersed for 1 year

increases remarkably with the appearance of nonlinearity of the P-V_M curves in both cases. At the maximum load, however, the AE activity for the immersed specimen is extremely low compared to that for the specimen without immersion. These experimental data suggest that the difference of the AE activity for the two specimens is due to the different microfracture processes.

Figure 10 shows the relationship between the accumulated AE energy ΣE_{AE} and the stress intensity factor K_ρ for the specimen without immersion. It is recognized from this figure that the relationship between $\log(\Sigma E_{AE})$ and $\log(K_\rho)$ is expressed by two linear relationships, and that the accumulated AE energy ΣE_{AE} begins to increase abruptly at a load designated by the change of the slope. A similar relationship was obtained for the specimens immersed in distilled water. The abrupt increase of ΣE_{AE} corresponds to the rapid extension of the microfractured region because the AE signals correspond to the microfractures that are due to resin cracking, fiber debonding and fiber breakage[7]~[9]. The results of the fracture toughness $K_{\rho,AE}$ which is defined as the critical stress intensity factor designated by the change of the slope, are shown in Table 1. The value of $K_{\rho,AE}$ is 16.9MPa·m$^{1/2}$ for the specimen without immersion, and decreases with increasing immersion time. The values of the fracture toughness $K_{\rho,Q}$ obtained by the 5% offset procedure of ASTM standard E 399[5] and the normalized average weight of water in the circle adjacent to the crack tip $\hat{C}/C_s$ are also shown in Table 1. As can be seen, the value of $K_{\rho,Q}$ decreases with

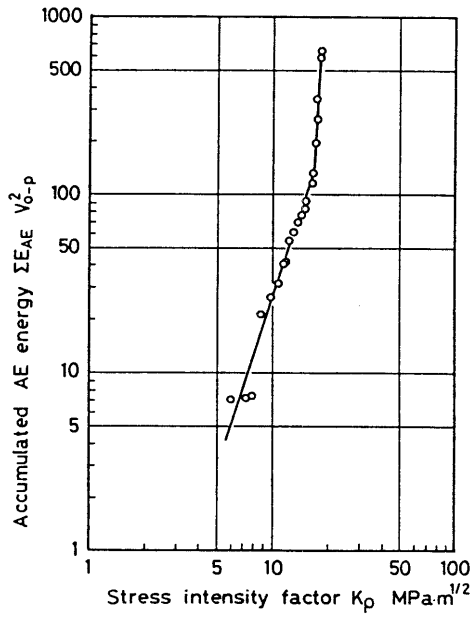

Fig. 10 ΣE_{AE}-K_ρ diagram for the specimen without immersion

Table 1 Results of fracture toughness $K_{\rho,AE}$ and $K_{\rho,Q}$ and $\hat{C}/C_s$

Condition	$K_{\rho,AE}$ MPa·m$^{1/2}$	$K_{\rho,Q}$ MPa·m$^{1/2}$	$\hat{C}/C_s$
Without immersion	16.9	17.4	
Immersion during 10 days	15.0	15.0	0.694
30 days	13.0	13.1	0.777
60 days	11.8	12.1	0.812
90 days	11.9	12.0	0.832
1 year	8.5	8.9	0.874
1.5 years	9.5	7.6	0.886

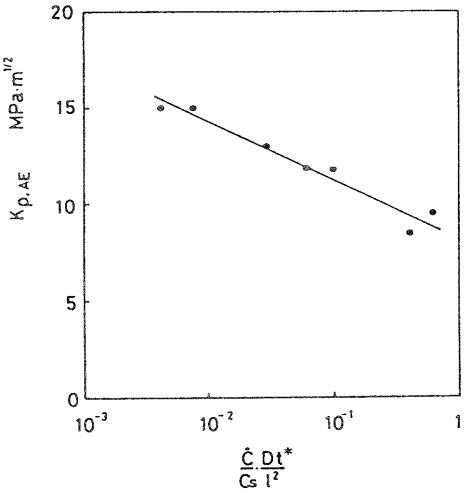

Fig. 11 Relationship between fracture toughness $K_{\rho,AE}$ and parameter $(\hat{C}/C_s)\cdot(Dt^*/l^2)$

(a)

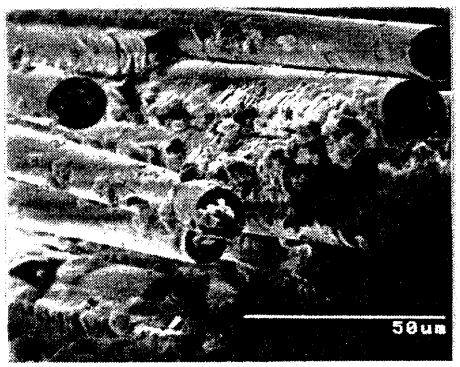

(b)

Fig. 12 Fractographic observation near notch tip of the specimen without immersion

increasing value of $\hat{C}/C_s$. Moreover, the value of fracture toughness $K_{\rho,AE}$ due to the AE method agrees satisfactorily with that of $K_{\rho,Q}$.

In order to discuss quantitatively the effect of water on the fracture toughness, the relationship between the fracture toughness $K_{\rho,AE}$ and a parameter which is the product of the normalized average weight of water $\hat{C}/C_s$ and the normalized immersion time Dt^*/l^2 is shown in Fig. 11. This figure reveals that the fracture toughness $K_{\rho,AE}$ has a linear relationship to $\log[(\hat{C}/C_s)\cdot(Dt^*/l^2)]$. As a consequence, the value of the fracture toughness at any immersion time can be estimated by using Figs. 6 and 11.

The fractured surfaces were observed by a scanning electron microscope. The typical examples of the fractured surfaces for the specimen without immersion and that immersed for 1 year are shown in Figs. 12 and 13, respectively. By comparing with the fractured surfaces, the fact that the fracture toughness and the number of the AE events detected during the tests reduce due to water can be qualitatively interpreted.

Figure 12(a) shows the fractured surface near the notch tip of the specimen without immersion. Pull-out fibers parallel to or aslant the surface are observed. Figure 12(b) is the enlarged picture by SEM. It is seen from this figure that many pieces of the unsaturated polyester resin adhere to the fiber surface. From this observation, the microfracture process of the specimen without immersion could be considered as follows: The matrix resin around the fiber bundles is cracked at first, and then the fibers which accompany the matrix resin are pulled out.

On the other hand, the fiberpull-out length of the specimen immersed in water for 1 year is shorter than

Table 2 Chemical composition of glass fiber (wt. %)

	Chemical composition wt%
SiO_2	52 ~ 56
Al_2O_3	12 ~ 16
CaO	15 ~ 25
MgO	0 ~ 6
B_2O_3	8 ~ 13
K_2O, Na_2O	< 0.8

Table 3 Result of quantitative analysis for the dissolution elements

Elements	Concentration ppm
Si	0.13
Al	–
Ca	0.028
Mg	0.0033
B	–
K	0.030
Na	0.051

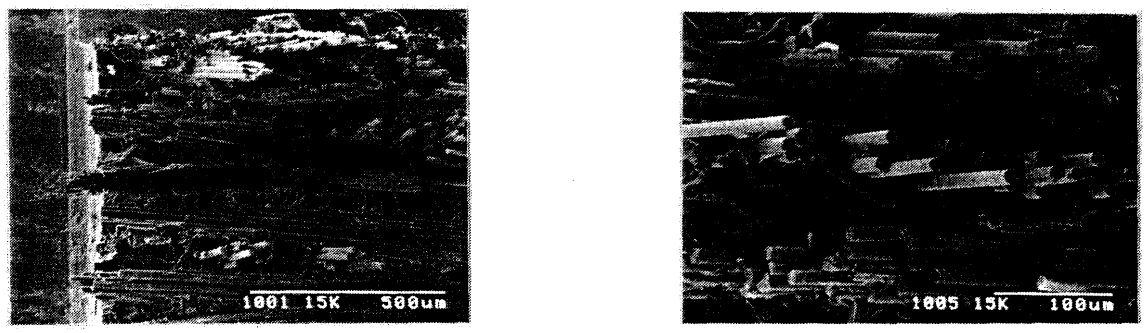

(a) (b)

Fig. 13 Fractographic observation near notch tip of the specimen immersed for 1 year

that of the specimen without immersion, as shown in Fig. 13(a). Figure 13(a) shows the enlarged picture of the pull-out fibers. Few pieces of matrix resin are observed on the surfaces of the pull-out fiber bundles. This indicates that the absorbed water reduces the adhesive strength between fiber and matrix resin. Therefore, the difference of the AE activity between the specimen without immersion and the immersed specimens could be explained by the degradation of the strength of the bonding interface between fibers and matrix resin, and the weakening of the strength of those fibers.

In order to discuss the effect of the environmental history on the fracture toughness, a fracture toughness test was carried out. The specimen was prepared by drying in a desiccator at room temperature after being immersed in distilled water for 30 days. The number of the AE events for the dried specimen is almost the same as that for the specimen immersed for 30 days and not dried. The fracture toughness for the dried specimen was obtained as $K_{\rho,AE}=14.4$ MPa·m$^{1/2}$. This value is also close to that for the specimen immersed for 30 days. Therefore, in the case of drying the specimen, the fracture toughness does not return to the state of the specimen without immersion. This fact suggests that the degradation of the FRP due to water is an irreversible change.

5. Degradation Mechanism Due to Water

The degradation of the FRP in water can be classified into four types, i. e., physical degradation such as "swelling", degradation of matrix resin due to chemical reaction with water, degradation of bonding interfaces between fibers and matrix resin due to hydrolysis of the coupling agent on the surfaces of glass fibers, and weakening of the strength of glass fibers due to the dissolution of metal oxide in water.

To clarify the degradation mechanism of the FRP in water, the quantitative analysis of dissolution elements from the specimen immersed for 90 days was performed by using an atomic absorption spectrophotometer. This analysis was made for the elements Si, Al, Ca, Mg, B, K and Na of which the glass fiber consists. The chemical composition of the glass fiber is given in Table 2. The analysis for the element Si was performed by graduating the solution by 1/20, and for the other elements by 1/10. The result is shown in Table 3. It is seen from Table 3 that small quantities of Si, Ca, Mg, K and Na are detected. This indicates that the elements move from the glass fibers to water by an ion exchange reaction[15][16], such that

$$Si-O-Na+H^+OH^- \longrightarrow Si-O-H+Na^+ +OH^-$$

Large quantities of Na and K were detected in the water, in spite of their low content relative to the elements Al, Ca, Mg and B in the glass fiber. This was

viewed as a result of their higher solubility in water. This suggests that the strength of the glass fiber may be weakened by the formation of microscopic defects due to the dissolution of metal oxides in water.

Finally, it is concluded that the strength deterioration of the FRP in water is caused by the degradation of bonding interfaces between fibers and matrix resin and the weakening of the strength of glass fibers.

6. Conclusions

Fracture toughness tests were performed by means of the AE method for a random short-fiber sheet molding compound composite in water. The fractographic observation of the fractured surfaces and the quantitative analysis of dissolution elements from the FRP were also carried out. The effect of water on the fracture toughness and the degradation mechanism due to water were discussed. The main results are summarized, as follows: (1) The maximum load and the fracture toughness decrease with increasing water immersion time; (2) The number of the AE events also decrease with increasing immersion time; (3) The fracture toughness $K_{\rho,AE}$ decreases linearly with increasing parameter log $[(\tilde{C}/C_s)\cdot(Dt^*/l^2)]$. (4) The strength deterioration is caused by the degradation of bonding interfaces between fibers and the matrix resin, and the weakening of the strength of glass fibers.

References

(1) Masuda, Y., Yamazaki, J., Ihara, F. and Narasaki, N., Trans. Jpn. Soc. Mech. Eng., (in Japanese), Vol. 44, No. 380 (1978-4), p. 1103.

(2) The society of Japanese Aerospace Co., Inc., Report of Investigation into Developments of Advanced Aircrafts Technology, (in Japanese), No. 604, (1982), p. 44.

(3) Owen, M. J. and Cann, R. J., J. Mater. Sci., Vol. 14, No. 8 (1979), p. 1982.

(4) Garg, A. C. and Trotman, C. K., Eng. Fract. Mech., Vol. 13, No. 2 (1980), p. 357.

(5) ASTM standards E 399-81, Annual Book of ASTM Standards, Vol. 10 (1980), p. 592, American Society for Testing and Materials.

(6) Suzuki, M., J. Jpn. Soc. Compos. Mater., (in Japanese), Vol. 7, No. 3 (1981), p. 88.

(7) Sekine, H., Shimomura, K., Takahashi, H. and Fujino, K., lst Int. Symp. Acoust. Emission from Reinforced Composites, S 3 (1983), p. 1, Soc., Plastics Industry.

(8) Shimomura, K., Sekine, H., Takahashi, H., Kishimoto, H., Suzuki, M. and Fujino, K., J. NDI, (in Japanese), Vol. 33, No. 7 (1984-7), p. 520.

(9) Sekine, H. and Ozawa, Y., Progress in Acoustic Emission II, (1984), p. 488, Jpn. Soc. Non-Destructive Inspection.

(10) Okuda, S., Reinforced Plastics, (in Japanese), Vol. 29, No. 3 (1983), p. 95.

(11) Noble, B., Harris, S. J., and Owen, M. J., J. Mater. Sci., Vol. 18, No. 4 (1983), p. 1244.

(12) Niitsuma, H., Chubachi, N., Sato, R., Takahashi, H. and Mori, Y., J. NDI, (in Japanese), Vol. 30, No. 11 (1981-11), p. 886.

(13) Nomura, Y., Applied Mathematics, (in Japanese), (1982), p. 177, Uchidarokakuho.

(14) Carslaw, H. S. and Jaeger, J. C., Conduction of Heat in Solids, (1959), Oxford.

(15) Hogg, P. J. and Hull, D., Developments in GRP Technology-1, (1983), p. 37, Applied Science Publishers.

(16) Tsuchihashi, S., Chemistry of Glass, (in Japanese), (1985), p. 145, Kodansha.